Accepted Manuscript

Functional Materials Letters

Article Title:	A facile synthesis of carbon-encapsulated $ZnFe_2O_4$ nanocrystals as anode for lithium-ion batteries
Author(s):	Boyang Liu, Shuyu Ke, Xiqin Zhang, Shuang Cai, Yingfeng Shao, Qi Yu, Shengchang Yan
DOI:	10.1142/S1793604719500292
Received:	22 October 2018
Accepted:	15 November 2018
To be cited as:	Boyang Liu *et al.*, A facile synthesis of carbon-encapsulated $ZnFe_2O_4$ nanocrystals as anode for lithium-ion batteries, *Functional Materials Letters*, doi: 10.1142/S1793604719500292
Link to final version:	https://doi.org/10.1142/S1793604719500292

World Scientific
www.worldscientific.com

Functional Materials Letters
Vol. 1, No. 1 (2015) 1–4

A facile synthesis of carbon-encapsulated $ZnFe_2O_4$ nanocrystals as anode for lithium-ion batteries

Boyang Liu, *[1] Shuyu Ke,[1] Xiqin Zhang,[1] Shuang Cai, [1] Yingfeng Shao, [2] Qi Yu, [1] and Shengchang Yan[1]
[1] *College of Ocean Science and Engineering, Shanghai Maritime University, Shanghai 201306, China*
[2] *State Key Laboratory of Nonlinear Mechanics, Institute of Mechanics, Beijing 100190, China*
byliu@shmtu.edu.cn
shaoyf@lnm.imech.ac.cn

Received Day Month Year; Revised Day Month Year

An explosive reaction between zinc nitrate hexahydrate and ferrocene taking place below 200 °C is discovered, which is employed for the one-step preparation of carbon-encapsulated $ZnFe_2O_4$ nanocrystals ($ZnFe_2O_4$@C) with core-shell structure in an autoclave. The small-sized equiaxed $ZnFe_2O_4$ nanocrystals have a median diameter of 22.1 nm. The uniform carbon shell of about 5 nm in thickness is amorphous, and its content is 32.6 wt.% in the nanocomposite. After 50 cycles, the $ZnFe_2O_4$@C anode still maintains a high specific capacity of 551 mAh g^{-1} at a current density of 50 mA g^{-1}. The efficient, energy-saving and environment-friendly method will be much attractive for preparing carbon-encapsulated different kinds of nanocrystals.

Keywords: Carbon-encapsulated $ZnFe_2O_4$ nanocrystals; Explosive reaction; Lithium-ion batteries.

Nanostructured zinc ferrite ($ZnFe_2O_4$) with a standard spinel structure and diverse morphologies has intriguing photocatalytic, catalytic, optical and magnetic properties, showing promise applications in various fields of catalysis, sensor, environmental remediation, drug delivery, actuator, and magnetic resonance imaging.[1] It is also an alternative eco-friendly anode material for the lithium-ion batteries (LIBs) because of its approximately three times larger theoretical capacity than the commercial graphite as well as the safe working voltage.[2] But for the pristine $ZnFe_2O_4$, the intrinsic low conductivity and large volume expansion during lithiation/delithiation process result in the poor high-rate capability and unsatisfied cycling performance. In order to solve these issues, a variety of nanometer-sized $ZnFe_2O_4$ structures are designed to reduce the lithium-ion-diffusion distance, which is beneficial for the rate performance. Additionally, the combination of carbon nanomaterials with good conductivity is widely recognized as an effective strategy for accommodating the volume expansion of $ZnFe_2O_4$ and enabling the long cycling life.[3-4] Consequently, Carbon-encapsulated $ZnFe_2O_4$ nanocrystals ($ZnFe_2O_4$@C) with core-shell structure and enhanced electrochemical performance is considered as a superior anode for LIBs.

In the past decade, considerable efforts have been devoted to developing new strategies for the preparation of $ZnFe_2O_4$@C. Since the reaction mechanism and the common synthetic route for $ZnFe_2O_4$ and carbon is quite different, it is difficult to simultaneously synthesize the $ZnFe_2O_4$@C. For example, The combustion, sol-gel, co-precipitation and hydrothermal methods carried out in an ambient atmosphere at relatively low temperature are generally employed to prepare $ZnFe_2O_4$ nanoparticles.[5] Nonetheless, carbon is conventionally obtained in an oxygen-free environment through thermal pyrolysis of organic precursors at a high temperature above 600 °C. Thus, the carbon coating is usually made on the already prepared $ZnFe_2O_4$ nanocrystals, implying that multistep and inefficient procedure is required.[6] The coating homogeneity is also hard to control especially for the scale-up fabrication. At present, the hydrothermal method is most frequently used for the one-step preparation of the $ZnFe_2O_4$@C owing to the feasibility of formation of carbon shell at a temperature as low as 200 °C via the polymerization and carbonization of glucose in solutions.[7] However, this time-consuming process restricts the practical applications of the $ZnFe_2O_4$@C.

Recently, we have proposed a universal oxidation approach for the one-step preparation of various of carbon-encapsulated metal sulfide/oxide nanocrystals with core-shell structure by the explosive reaction between metallocene compounds and ammonium persulfate (APS) below 200 °C in 30 mins.[8-11] Compared to the hydrothermal treatment, this method exhibits distinct advantages in terms of easy accessibility (without solution), short reaction time, lower reaction temperature and large-scale production. Hence, this attractive method is worthy to be deeply investigated so as to encapsulate more kinds of interior cores.

Considering that the nitrates are typical oxidizing agents in explosives where the rapid oxidation of carbon compounds takes place, zinc nitrate hexahydrate ($Zn(NO_3)_2{\cdot}6H_2O$) is as likely to react with ferrocene (Cp_2Fe) as APS. Based on this

assumption, these two substances are used as reactants in this paper, and $ZnFe_2O_4$@C is efficiently achieved as anticipated and its electrochemical performance as an anode for LIBs is evaluated either. The first successful preparation of binary metal oxide cores by our oxidation method allows further extending this approach for different core-shell structures.

The synthesis process is considerable simple and easy to handle. Typically, 10 mmol of Cp_2Fe and 5 mmol of $Zn(NO_3)_2{\cdot}6H_2O$ were mixed and placed into a 50 mL autoclave, which was hold at 200°C for 30 min. After cool down to room temperature, the as-obtained powder was cleaned by ethanol and dried at 100 °C. The phase structure, morphology, microstructure, and composition of the sample were studied by X-ray diffractometer (XRD), Raman spectrometer, scanning electron microscope (SEM) with an X-ray energy-dispersive spectroscope (EDS) and transmission electron microscope (TEM). Differential scanning calorimetric (DSC) and thermogravimetric (TG) analysis were recorded by a thermal analyzer.

The mixture of $ZnFe_2O_4$@C, polyvinylidene difluoride and acetylene black in a weight ratio of 8:1:1 was well dispersed in N-methyl-2-pyrrolidone. Then, the slurry was coated on the copper foil and vacuum dried at 120 °C for the coin cell anode. Lithium foil, microporous polypropylene membrane and 1.0 M $LiPF_6$ in EC/EMC (50:50) were used as the counter electrode, separator, and electrolyte, respectively. The cell cycling performance was investigated by a Neware battery tester between 0.01 and 3 V. The cyclic voltammogram (CV) was measured by an electrochemical workstation (CHI 630A) in 0.01-3 V at 0.05 mV s^{-1}.

The as-prepared black powder is a magnetic susceptible material, which is rapidly attracted under a magnet (Supplementary data, Fig. S1). The entire sharp diffraction peaks in the XRD pattern are well indexed to the cubic-spinel phase $ZnFe_2O_4$ (Fig.1a). The small broad peak between 20-30° indicated by the arrow is corresponding to the amorphous carbon, which is evidently revealed in the Raman spectrum (Fig. 1b). The D-band arising from the disordered carbon is almost equal in intensity to the G-band, further demonstrating that the carbon shell is amorphous. The diffusion rate of carbon atoms should be too sluggish at the low synthesis temperature to grow long-range ordered carbon shell. The SEM image in Fig. 1c displays that the powder is constituted of equiaxed and rod-like nanoparticles. The core-shell structure is proved by the transparent layer and the interior nanocrystals in the high-magnification image (Fig. 1d). The EDS spectrum in Fig. 1e shows that only C, O, Zn and Fe elements associated with the $ZnFe_2O_4$@C are found in the sample. The carbon content is 32.6 wt.%, determined by the weight loss of the sample in air from the TG curve (Fig. 1f).

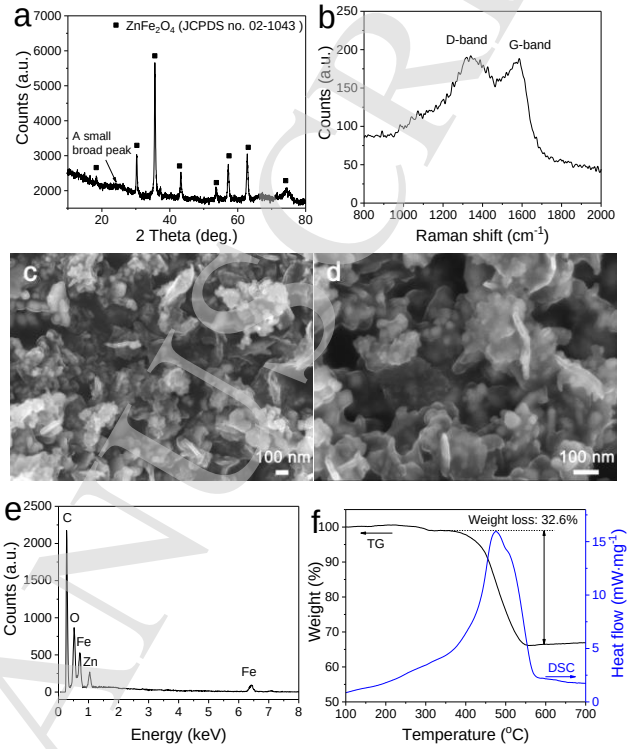

Fig. 1. (a) XRD pattern, (b) Raman spectrum, (c, d) SEM images, (d) EDS spectrum and (f) DSC-TG curves of the $ZnFe_2O_4$@C.

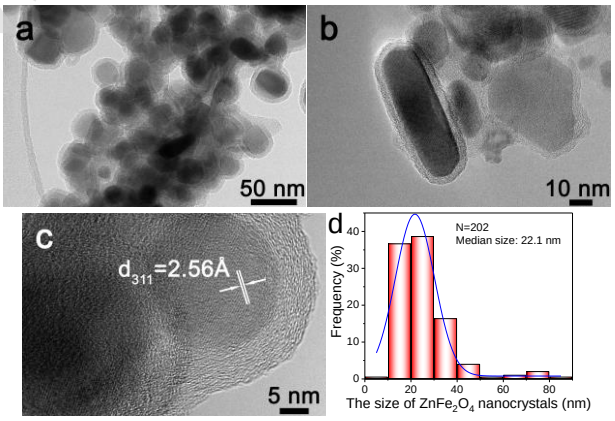

Fig. 2. (a, b, c) TEM images of the $ZnFe_2O_4$@C at different magnifications. (d) The size distribution of the equiaxed $ZnFe_2O_4$ nanocrystals.

The core-shell structure is obviously observed in the TEM image of Fig. 2a. The equiaxed nanocrystals are evenly and tightly surrounded by a carbon shell of *ca.* 5 nm in thickness. In addition, a small amount of slightly elongated nanocrystals can be found in Fig. 2b, which is in accordance with the SEM result. It is suggested that the atmosphere in some local area of the autoclave are suitable for the preferential growth of $ZnFe_2O_4$. The carbon shell is amorphous as proved by the disordered fringes on an individual $ZnFe_2O_4$ core in the high-resolution image (Fig.

2c). The short reaction time and low temperature will suppress the grain growth of $ZnFe_2O_4$, leading to the formation of small-sized nanocrystals with a median size of 22.1 nm (Fig. 2d).

The reaction details of the starting powder are analyzed by DSC-TG curves in open and sealed pans, respectively. Fig. 3a shows that the endothermic peak of the DSC curve located at 52.9 °C is attributed to the melt of $Zn(NO_3)_2{\cdot}6H_2O$. With the temperature increase, the second endothermic peak starts at 130.0 °C, and the corresponding weight loss in the TG curve becomes apparent during this period (gray area), owing to the elimination of the hydrate water of $Zn(NO_3)_2{\cdot}6H_2O$ in a flow of N_2. When the temperature is elevated to 134.1 °C, a very sharp exothermic peak accompanying by a 44.4 % vertical weight drop can be found, illustrating that a large volume of heat and gases are yielded in the ultrafast and violent reaction, which is a typical explosive reaction. When the sealed pan is used, the peaks do not coincide with those in the open pan measurement except the melting point of $Zn(NO_3)_2{\cdot}6H_2O$ initiated at 34.5 °C (Fig. 3b). The exothermic peak with an onset point of 107.6 °C is very broad, meaning that the reaction is gradually completed. However, the explosive reaction is clearly late according to the sharp peak at 170 °C. Unlike that in the open pan, the intermediate products cannot quickly escape in the sealed pan, thereby reducing the reaction speed in an equilibrium-controlled reaction. But the explosive reaction still occurs in spite of the delay, which should be crucial for the formation of the $ZnFe_2O_4$@C.

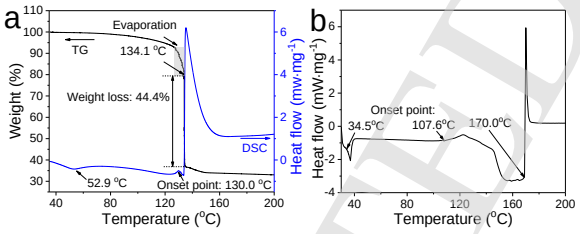

Fig. 3. DSC and TG curves of the reactants in different pans: (a) open; (b) sealed.

Fig. 4 shows the evolution of the synthesis process for the $ZnFe_2O_4$@C. Although Cp_2Fe is regarded as one of the most stable metallocenes, its sandwich structure composed of two parallel Cp ligands and the central Fe atom will be destructed under the attack of strong oxidants. As the temperature rises, $Zn(NO_3)_2{\cdot}6H_2O$ first melted down and impregnated into the solid Cp_2Fe powder, forming a uniform mixture as an explosive precursor. Then, nitrate radicals in the melted $Zn(NO_3)_2{\cdot}6H_2O$ began to oxidize the Cp_2Fe at 107.6 °C. The hydrogen atoms and unsaturated bonds in Cp ligands were stepwise abstracted and cleaved at the initial period, slowly releasing heat.[12] As the oxidation went on, a growing number of radicals formed and the mixture is highly reactive, resulting in a subsequent explosive reaction. The substantial heat was produced during the drastic oxidizing reaction, in which $ZnFe_2O_4$, carbon species and H_2O were produced. For comparison, the typical combustion process was usually carried out in an open crucible at ambient atmosphere.[2] $Zn(NO_3)_2{\cdot}6H_2O$ and $Fe(NO_3)_3{\cdot}9H_2O$ were intensively used together as oxidants, while the glycine ($C_2H_5NO_2$) or urea (CH_4N_2O) was supposed to coordinate to the nitrates and serve as the fuel. The carbon atoms in these fuels were oxidized to release large amounts of heat to sustain the combustion reaction, and the significantly increased temperature was higher for carbon oxidation. In addition, the carbon content in the fuels was much lower than that of Cp_2Fe, implying that carbon would completely transform to carbon oxides in the oxygen-rich environment rather than carbon shell. However, in our method, the carbon content in Cp_2Fe was as high as 64.5 wt.%, and the quantity of oxidant was limited in the sealed autoclave. Thus, the oxidant was largely consumed during the explosive reaction. Moreover, the reaction temperature was much lower than the oxidation temperature of amorphous carbon. Together with the short reaction time, the further oxidation of the small carbon species from the Cp ring was negligible, and the carbon species could be well retained on the $ZnFe_2O_4$ nanocrystals to in-situ form core-shell structure.[9] The low temperature and fairly short reaction time performed an adverse effect on the atomic diffusion and crystal growth, so amorphous carbon and small equiaxed $ZnFe_2O_4$ nanocrystals were eventually fabricated. The reaction equation was also proposed as follows. It can discover that no contaminative element is included in the reaction, meaning that the laborious purification procedure for the final product is dispensable. The mass production is able to be accomplished just depending on the quantity consumption and uniformity of the reactants. Therefore, this efficient, energy-saving and environment-friendly method will be much attractive in future for preparing carbon-encapsulated different kinds of nanocrystals.

$$(C_5H_5)_2Fe + Zn(NO_3)_2{\cdot}6H_2O \rightarrow ZnFe_2O_4@C + N_2 + H_2O$$

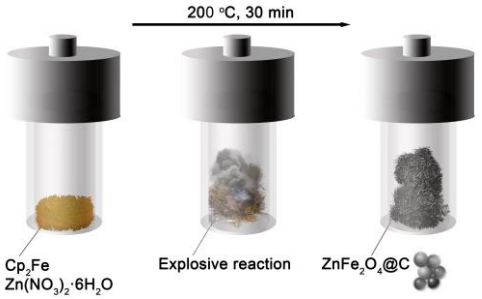

Fig. 4. The schematic of the synthesis of the $ZnFe_2O_4$@C.

The electrochemical properties of the $ZnFe_2O_4$@C anodes with a mass loading about 2 mg cm^{-2} are provided in Fig. 5. The sharp reduction peak at 0.75 V in the initial CV curve of Fig. 5a is ascribed to the formation of iron and zinc nanoparticles embedded in an amorphous Li_2O matrix in the lithiation process.[13] The corresponding reaction can be depicted as well by the long voltage plateau at *ca.* 0.8V in first discharge curve at 50 mA g^{-1} (Fig. 5b). The broad peak in the charge curve at about 1.7 V is derived from the oxidation of the metal nanoparticles. Thus, the major reaction is considered to be: $ZnFe_2O_4 + 8Li \leftrightarrow Zn + 2Fe + 4Li_2O$. In the following two cycles, the almost resembled curves are a feature of good cycling stability of $ZnFe_2O_4$@C and show a pronounced redox couple around 1.2/1.5 V, which can be assigned to the conversion reaction of Zn^{2+}, Fe^{3+}, and Fe^{2+} to Fe^0 and Zn^0. The first discharge and charge capacity of $ZnFe_2O_4$@C is 1171 and 797 mAh g^{-1}, respectively (Fig. 5b). The initial reversible capacity is 68 % as a result of the mass existence of amorphous carbon shell and the formation of solid electrolyte interface (SEI) film on the $ZnFe_2O_4$@C.

The cycling properties of the $ZnFe_2O_4$@C and pristine $ZnFe_2O_4$ under different current densities are illustrated in Fig. 5c. The discharge capacity of the $ZnFe_2O_4$@C anode is as high as 1171 mAh g^{-1} at 50 mA g^{-1} in the first cycle and becomes stable after five cycles. A specific capacity of 551 mAh g^{-1} can be kept after 50 cycles, indicating a good cyclic capacity retention. The specific capacity may be a bit lower than that of some report because the total weight of the $ZnFe_2O_4$@C anode is used rather than the individual $ZnFe_2O_4$.[14] At high current densities, a capacity of 510, 444, 385 and 241 mAh g^{-1} after 50 cycles is achieved at 100, 200, 500 and 1000 mA g^{-1}, respectively. However, for the pristine $ZnFe_2O_4$, although the initial capacity can reach to 1092 mAh g^{-1}, it degrades fast to 421 mAh g^{-1} in the first ten cycles and further decreases to 198 mAh g^{-1} at 50th cycle. Therefore, the carbon shell can greatly enhance the microstructure stability of the $ZnFe_2O_4$ anode during the charge/discharge process. The rate capability of the $ZnFe_2O_4$@C is also evaluated by stepwise increasing the current density from 100 to 1000 mA g^{-1}, as shown in Fig. 5d. The capacity vertically drops off as the current is raised and remains stable in the next twenty cycles. It still delivers a reversible capacity of 299 mAh g^{-1} at 50 mA g^{-1} even in the 90th cycle. When the current density changes back to 1000 mA g^{-1}, the capacity of the $ZnFe_2O_4$@C returns to 604 mAh g^{-1} at once and stabilizes in the following cycles. In summary, the carbon encapsulation can notably improve the cycling and rate performance of the $ZnFe_2O_4$.

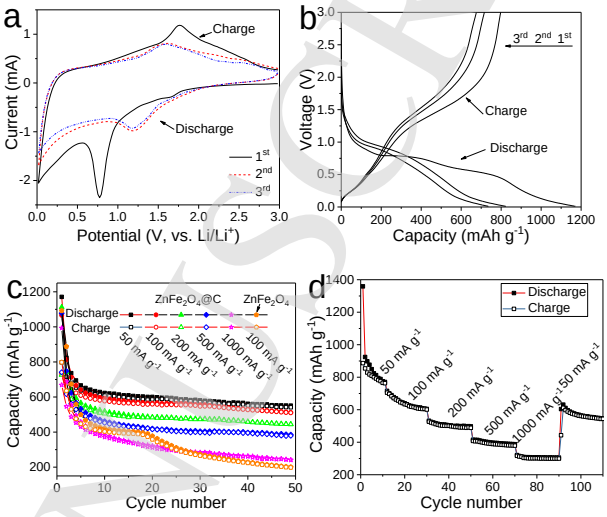

Fig. 5. Electrochemical performance of the $ZnFe_2O_4$@C: (a) CV curves in the first three cycles; (b) The first three charge/discharge curves at 50 mA g^{-1}; (c) Cycling properties under different current density; (d) Rate capability.

In conclusion, $Zn(NO_3)_2 \cdot 6H_2O$ is an effective oxidant to explosively react with Cp_2Fe at low temperature, and the $ZnFe_2O_4$@C can be directly obtained when the reaction is carried out in an autoclave. As an anode material, the $ZnFe_2O_4$@C with core-shell structure has good cycling and rate performance. The simple and efficient method is suited for scalable preparation of core-shell structures.

Acknowledgement

This work is supported by Natural Science Foundation of Shanghai (18ZR1417000), National Natural Science Foundation of China (11572326) and Opening fund of State Key Laboratory of Nonlinear Mechanics.

References

(1) J. Zhang, *et al. Sensor. Actuat. B Chem.* **221**, 55 (2015).
(2) H. Yue, *et al. Electrochim. Acta* **180**, 622 (2015).
(3) Y. An, *et al. Funct. Mater. Lett.* **9**, 1642008 (2016).
(4) Z. Zhang, *et al. Materials Technology* **31**, 497 (2016).
(5) P. A. Vinosha, *et al. Optik* **134**, 99 (2017).
(6) D. Bresser, *et al. Advanced Energy Materials* **3**, 513 (2013).
(7) H. Wang, *et al. Energy Technology* **5**, 611 (2017).
(8) B. Liu, *et al. Nanotechnology* **27**, 075603 (2016).
(9) B. Liu, *et al. Carbon* **127**, 21 (2018).
(10) B. Liu, *et al. Carbon* **68**, 573 (2014).
(11) Y. Zhou, *et al. Funct. Mater. Lett.* **11**, 1850008 (2018).
(12) J. Noda, *et al. Phys. Chem. Chem. Phys.* **2**, 2555 (2000).
(13) Y. Sharma, *et al. Electrochim. Acta* **53**, 2380 (2008).
(14) L. Yao, *et al. J. Power Sources* **258**, 305 (2014).

Supplementary data

A facile synthesis of carbon-encapsulated $ZnFe_2O_4$ nanocrystals as anode for lithium-ion batteries

Boyang Liu, *[1] Shuyu Ke,[1] Xiqin Zhang,[1] Shuang Cai, [1] Yingfeng Shao, [2] Qi Yu, [1] and Shengchang Yan[1]

[1] *College of Ocean Science and Engineering, Shanghai Maritime University, Shanghai 201306, China*

[2] *State Key Laboratory of Nonlinear Mechanics, Institute of Mechanics, Beijing 100190, China*

Corresponding authors:

1. Boyang Liu

   Email: byliu@shmtu.edu.cn

   Tel.: +86-21-38284803, Fax: +86-21-38284818

2. Yingfeng Shao

   E-mail address: shaoyf@lnm.imech.ac.cn

   Tel.: +86-10-82544360.

The optical photograph of the as-prepared powder in the ethanol is presented in Fig. S1. When bring a magnet near the centrifuge tube, the powder was quickly got attracted to the magnet, demonstrating that the powder has good magnetic responsibility.

Fig. S1. The as-prepared powder dispersed in ethanol was attracted by a magnet.

The enlarged image of Fig. 2c is shown in Fig. S2. The lattice fringes are clearly shown in this image, which can be indexed to the (311) plane of cubic-spinel phase $ZnFe_2O_4$.

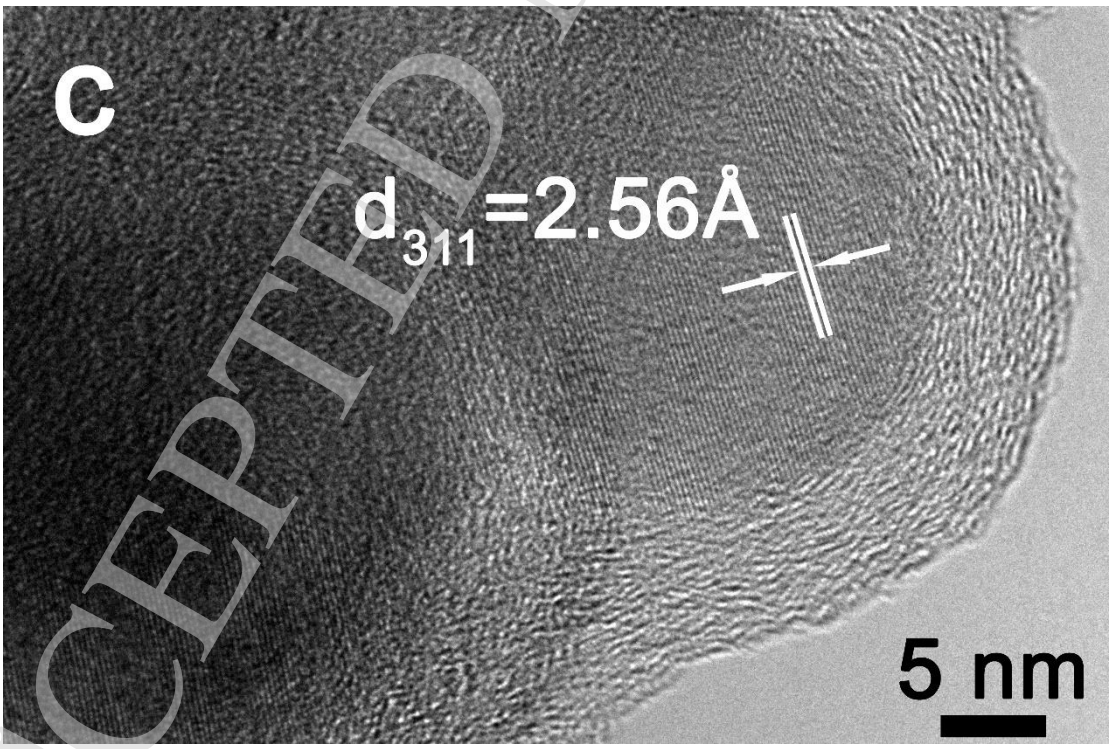

Fig. S2. The enlarged image of Fig. 2c.